HHS Public Access

Author manuscript

Curr Opin Solid State Mater Sci. Author manuscript; available in PMC 2024 July 31.

Published in final edited form as:

Curr Opin Solid State Mater Sci. 2024 June ; 30: . doi:10.1016/j.cossms.2024.101147.

Advancements in fluorescence lifetime imaging microscopy Instrumentation: Towards high speed and 3D

Jongchan Park, **Liang Gao***

Department of Bioengineering, University of California, Los Angeles, CA 90025, USA

Abstract

Fluorescence lifetime imaging microscopy (FLIM) is a powerful imaging tool offering molecular specific insights into samples through the measurement of fluorescence decay time, with promising applications in diverse research fields. However, to acquire two-dimensional lifetime images, conventional FLIM relies on extensive scanning in both the spatial and temporal domain, resulting in much slower acquisition rates compared to intensity-based approaches. This problem is further magnified in three-dimensional imaging, as it necessitates additional scanning along the depth axis. Recent advancements have aimed to enhance the speed and three-dimensional imaging capabilities of FLIM. This review explores the progress made in addressing these challenges and discusses potential directions for future developments in FLIM instrumentation.

Keywords

Fluorescence lifetime; Bioimaging; High speed imaging; 3D imaging; Microscopy

1. Introduction

Fluorescence lifetime imaging microscopy (FLIM) has found extensive utility across a broad spectrum of scientific domains, spanning materials science, biology, and medicine [1–10]. Unlike traditional intensity-based methods, FLIM doesn't simply capture time-integrated fluorescent signals; rather, it focuses on the temporal aspects of fluorescent decay (Fig. 1a). The fluorescence lifetime, which hinges on the molecular environment of a fluorophore within materials or living organisms rather than its concentration, endows FLIM with the capability to enable more precise and quantitative analyses of molecular effects.

FLIM techniques can be broadly categorized into two main types: frequency-domain FLIM [11] and time-domain FLIM [12,13]. Frequency-domain FLIM employs modulated light at a particular frequency to illuminate the sample, provoking fluorescence with the same frequency but distinct modulation depth and phase shift due to non-instantaneous decay (Fig. 1b). By modulating the camera gain at the identical or slightly different frequency

*Corresponding author. gaol@ucla.edu (L. Gao).

Declaration of competing interest

The authors declare that they have no known competing financial interests or personal relationships that could have appeared to influence the work reported in this paper.

as the excitation light, frequency-domain FLIM can extract phase shifts and modulation depths from the fluorescence signals, allowing the fluorescence lifetime to be determined by comparing these measurements with a reference fluorophore of known lifetime. In contrast, time-domain FLIM relies on pulsed laser excitation to illuminate the sample, followed by sequential measurements of fluorescent decay in discrete time channels utilizing an ultrafast detector or detector array (Fig. 1c). Owing to its direct measurement of transient fluorescence signals, time-domain FLIM provides more detailed information about decay dynamics (Fig. 1c) than its frequency-domain counterpart. This feature proves especially valuable when dealing with complex fluorophores exhibiting multiple decay components. Additionally, when operating in the photon counting mode, time-domain FLIM can work with signals at extremely low intensities such as from single molecules while frequency-domain FLIM working under analog recording generally requires a much higher photon flux [14].

Despite their widespread applications, conventional FLIM technologies have two significant drawbacks. First, they grapple with slow imaging speeds. Traditional FLIM systems scans the sample both in the spatial and temporal domain, to generate lifetime maps. However, these methods usually face challenges in swiftly acquiring data, rendering them inadequate for capturing fast dynamic events. Second, conventional FLIM imaging is predominantly confined to two dimensions. The lack of three-dimensional (3D) imaging capabilities restricts its utility when dealing with samples featuring complex structures. In this review, we discuss the recent strides made in FLIM instrumentation, with a particular focus on mitigating these two constraints. In our opinion, these developments represent the cutting edge of research in this field, showcasing exciting progress that is reshaping the landscape of FLIM.

2. Dimensionality gap in FLIM measurement

The conventional FLIM systems encounter difficulties in achieving faster frame rates and imaging beyond 2D due to what is often referred to as the “dimensionality gap”. In contrast to intensity-based methods, FLIM relies on image sensors with ultrashort impulse response functions, typically in the nanosecond or picosecond range, to accurately capture transient fluorescence decay events. These ultrafast photodetectors are often limited to low-dimensional formats, like 0D (point detectors) or 1D (linear detector arrays), primarily due to the complexities and cost associated with their fabrication. When using such low-dimensional photodetectors to measure high-dimensional (2D or 3D) FLIM images, extensive scanning along other spatial dimensions often becomes necessary.

Additionally, FLIM records the time-resolved fluorescence decay at each scanning location, resulting in significantly longer pixel/line dwell times compared to intensity-only measurements. For instance, in a confocal microscope, capturing a 512×512 pixel image with a 1 μs pixel time takes a frame time of a fraction of a second. However, for FLIM measurements, the pixel dwell time must be extended because the detected photons are distributed across different temporal bins. To achieve the same average signal-to-noise ratio (SNR) across all temporal bins as that of a confocal microscope, which temporally integrates all light signals, FLIM must increase the pixel dwell time by a factor of N, where N is the

number of temporal bins. This often leads to a frame time extending to several minutes. The challenge is further exacerbated in 3D imaging, as it requires additional scanning along the depth axis, compounding the time required for comprehensive data acquisition.

While it is possible to mitigate the prolonged scanning dwell time to some extent by increasing the excitation intensity, this approach comes with the drawback of elevated photobleaching and phototoxicity to the sample [15]. Furthermore, when fluorophores reach their saturation states [16] – a point at which additional increments in excitation intensity fail to induce more fluorescence, a scenario frequently encountered in confocal systems – even this strategy becomes ineffective. This method is also futile when the incident photon rate has already surpassed the counting capacity of a photon-counting FLIM system, which is determined by the dead times of the photodetector and timing electronics and typically falls in the MHz range [17].

3. Advances in high-speed FLIM

Two strategies have been employed to enhance the speed of FLIM. The first strategy involves reducing scanning dwell time by elevating the photon count rate or utilizing analog recording. In the measurement of fluorescence lifetime, a time-domain FLIM imager can operate in either time-gated or time-correlated single photon counting (TCSPC) mode, with TCSPC being the preferred detection method due to its higher precision, faster speed, and increased sensitivity [18,19]. In order to minimize the scanning dwell time in the TCSPC mode, it is crucial to maximize the average photon counting rate at each scanned position, which can be expressed as [17]:

$$r_a = \frac{r_p \tau}{2T}. \quad (1)$$

here r_p is the peak incident photon rate, τ is the fluorescence lifetime, and T is the excitation pulse period (also referred to as the signal window). To increase r_a, we can reduce T (*i.e.*, increase the excitation pulse rate) and/or raise r_p (i.e., increase the excitation pulse energy). However, the lower limit of T is determined by the photodetector's dead time and typically set to be greater than twice the fluorescence lifetime. Also, to avoid issues like pile-up effects and counting loss, the conventional practice is to set r_p at only a small fraction (typically < 5 % [20]) of the photodetector's maximum photon counting rate (the inverse of its dead time), leading to a reduced detection duty cycle and, therefore, a slow frame rate (Fig. 2a).

One solution to lift this limit on r_p is to split the light into several detector channels and employ parallel TCSPC modules. With parallel detection in FLIM systems, the pile-up effect is efficiently suppressed because photons lost by one detector can be potentially detected and timed by another detector in parallel. For instance, a state-of-the-art TCSPC-FLIM system with four parallel channels can capture a 256×256 pixel image in five seconds [21]. Another study demonstrated that a seven-channel TCSPC-FLIM system can reduce the pixel dwell

time by a factor of 2.5 compared to a conventional single-channel system while acquiring a similar number of photons [22] (Fig. 2b).

Alternatively, the fluorescence decay waveform can be continuously measured by a time-domain analog-recording technique. In this approach, the detected light signals are directly recorded by a fast-digitalizing device, bypassing traditional photon-counting electronics. The shape of the recorded signal no longer resembles the actual fluorescence decay due to limitations in the temporal resolution of the photodetector. However, the delay between the centroid of the signal and a reference signal from the laser represents the apparent lifetime of the fluorescence decay. Theoretically, analog recording is exempt from issues related to pile-up and counting loss. Therefore, there is no intrinsic limitation in incident photon rate or signal intensity. In practice, the recordable photon rate and recording speed are constrained by the linearity range and the maximum output current of the detector. Using this approach, it has been demonstrated that FLIM imaging with a resolution of 256×256 pixels can be achieved at a video rate (20 frames per second) [23,24](Fig. 2c, d). In another implementation, Karpf et al. enhanced the speed to kilohertz using spectro-temporal encoded illumination for rapid point scanning [25] (Fig. 2e). Nevertheless, these direct analog-recording techniques fall short in providing sub-nanosecond fluorescence lifetime estimations due to the relatively long impulse response function of photodetectors and are fundamentally constrained by the bandwidth of digitizers.

The second strategy facilitating fast FLIM involves parallel recording of fluorescence decay events across multiple spatial locations. Rather than measuring the fluorescence decay at a pixel or line at a time, these techniques capture 2D time-resolved snapshots of fluorescence scenes along the decay curve, thereby eliminating the need for spatial scanning when acquiring a plane image. However, conventional 2D ultrafast cameras like micro-channel plates often suffer from constrained pixel resolutions and entail substantial costs. Recent advancements in wide-field FLIM with single-photon avalanche diode (SPAD) arrays overcome these limitations by fabricating the device with standard complementary-metal-oxide semiconductor (CMOS) technology, resulting in more affordable prices and higher resolutions [26]. For example, Zickus et al. reported a 0.5-megapixel SPAD camera with acquisition rates up to 1 Hz [27,28] (Fig. 3a, b). Nonetheless, these high-resolution SPAD cameras are typically operated in a gated acquisition mode, which, compared to the TCSPC mode, offers a lower temporal resolution due to the physical constraints imposed by the necessity to incorporate complex timing electronics for each individual pixel on the same chip.

Rather than pursuing parallel acquisition at the device level, the simultaneous capture of multiple time-resolved fluorescence decay images can be accomplished at the system level as well. The crux of this technological approach lies in time-to-space mapping, typically through introducing a time-dependent spatial shifting to the fluorescence decay images and, thereby, allowing them to be measured by distinct segments of a camera or a camera array. The temporal resolution in this method is not governed by the intrinsic capabilities of the recording device but rather by the speed at which the system can execute image shifts. Therefore, the cameras utilized in this strategy typically do not necessitate 2D ultrafast imaging capabilities; they can instead be conventional time-integrated or gated cameras.

Building on this principle, Kapitany et al. developed a single-shot time-folded FLIM method [29] (Fig. 3c, d). They employed an optical cavity to generate temporally delayed and spatially sheared replicas of the fluorescent decay signal, directing them onto a time-gated intensified charged-coupled device. This configuration enabled the simultaneous sampling of different segments of the decay signal by a single camera. However, a drawback of their approach arises from signal loss occurring each time it passes through the beam splitter within the delay cavity. Consequently, the images captured along the decay curve exhibit a gradual decline in intensity, placing a constraint on the total number of parallel time-resolved fluorescence decay images it can effectively acquire.

In contrast, our research group introduced an approach known as Compressed Ultrafast Photography FLIM (CUP-FLIM) [30,31], employing compressed sensing to capture the complete fluorescence decay waveform in a single shot (Fig. 3e). In CUP-FLIM, we initiate the process by encoding the incident image with a random binary pattern using a digital micromirror device (DMD). Subsequently, we employ a streak camera, traditionally utilized as a line image sensor, to spatially shift the resulting time-lapse images. Unlike conventional use, we fully open the entrance slit of the streak camera, transforming it into a 2D image input receiver. The ultimately obtained spatially-sheared decay images are then temporally integrated at a standard charge-coupled device (CCD) image sensor. While the signals are initially mixed in the raw image, computational recovery is achievable, contingent upon the assumption that the fluorescence scene exhibits sparsity in the spatial gradient domain, specifically being piece-wise smooth. With CUP-FLIM, we demonstrated an imaging speed up to 100 Hz in fluorescence imaging, constrained only by the readout speed inherent to the streak camera (Fig. 3f, g).

Although CUP-FLIM facilitates rapid wide-field acquisition, its reliance on an expensive streak camera restricts its widespread adoption in typical biological laboratories. Addressing this limitation, Liu et al. devised a cost-effective alternative—single-shot compressed optical-streaking ultra-high-speed photography (COSUP) [32]. This method aligns with the core principle of CUP-FLIM but replaces the expensive streak camera with a rotating galvanometer mirror. This mirror introduces time-dependent spatial shifts to the time-lapse fluorescence decay images. The researchers successfully demonstrated the efficacy of their approach in luminescence lifetime imaging of upconverting nanoparticles within living cells at a video rate of 20 Hz [33]. However, it’s worth noting that the relatively slow rotation speed of galvo mirrors imposes a challenge, resulting in a lower lifetime resolution of approximately 30 microseconds.

Another alternative approach to achieve time-dependent spatial shifting is to use a fast polarization switch. For example, Bowman et al. developed an electro-optic FLIM (EO-FLIM) ratiometric method [34,35], employing Pockels cells to gate the fluorescence decay into two orthogonal polarization components. These polarized beams are then recombined at an angle through a polarization beam splitter and reimaged onto adjacent locations on a camera. The fluorescence lifetime can then be estimated through ratio of the resultant fluorescence intensities at these two locations. Using this method, they demonstrated a kilohertz FLIM of neural action potentials *in vivo* [36]. However, the measurement of only two temporal channels prevents their approach from capturing the entire fluorescence decay

curve. Consequently, its application is restricted when imaging fluorophores characterized by complex multi-exponential decay components.

4. Advances in 3D FLIM

To acquire a 3D FLIM image, conventional confocal FLIM technologies must scan along the additional depth axis, often leading to a prohibitively long acquisition time. To achieve a more practical acquisition time, it is essential to minimize the measurement dimensionality gap, as discussed in Section 2, through parallel detection.

An early implementation of this approach entails the integration of a time-gated camera with a Nipkow disk microscope [37,38]. This approach allows for simultaneous lifetime measurements at multiple spatial points. However, to construct a 2D FLIM image, the point array still requires scanning across the sample, leading to a 30-second acquisition time for a depth-resolved FLIM image with eight gated channels [37]. Unfortunately, at this rate, acquiring a 3D FLIM image becomes unfeasible. Subsequent efforts by the same research group enhanced the depth-resolved FLIM image rate to ten frames per second [39]. Nonetheless, this improvement came at the cost of a reduction in the number of gated channels.

To eliminate the need for in-plane scanning and accelerate 3D image acquisition, recent efforts involve integrating structured illumination like light-sheet with wide-field FLIM imaging [40–44]. In this approach, the lifetimes of all in-plane spatial points are measured simultaneously, and the 3D FLIM rate is dictated by the camera exposure time and the number of scanning steps along the depth axis. For instance, employing a frequency-domain FLIM camera, Greger et al. showcased the capability to achieve 3D FLIM of a volume spanning 100 μm^3 within a mere minute [44]. In another notable implementation, Hirvonen et al. utilized a time-domain TCSPC FLIM camera, achieving full-waveform recording of fluorescence lifetimes with a volumetric frame time of just a few minutes [42] (Fig. 4a, b).

Acquiring a 3D FLIM image through depth scanning faces a fundamental trade-off between the number of depth scans and the volumetric frame rate. An alternative approach that bypasses this constraint is FLIM tomography [45], which acquires 2D projections of a 3D object at various angles using a widefield FLIM camera. The 3D fluorescence image at a specific time along the decay curve can then be computed through tomographic reconstruction. Using this method, McGinty et al. constructed a fluorescence lifetime optical projection tomography system and demonstrated its utility in imaging optically cleared samples [46] (Fig. 4c). Later, the same group extended their method to transparent living systems [47,48] (Fig. 4d). Because tomography typically requires rotation of the samples, the volumetric frame rate thus hinges on how fast the system can complete the angular measurement.

It is noteworthy that FLIM tomography operates fundamentally as a frequency-domain scanning technique. In contrast to confocal or light-sheet FLIM, which requires continuous spatial sampling for recovering full spatial resolution, FLIM tomography can potentially selectively measure a subset of frequency components within the object’s 3D power

spectrum [49]. This approach is especially effective when the sample exhibits sparsity in the spatial domain, allowing fewer measurements and faster processing speed while maintaining an optimal resolution.

Conventional FLIM tomography mandates sample rotation for angular measurements, posing challenges in precise sample positioning for microscopic imaging and consequently restricting its application mainly to macroscopy. To solve this problem, our group has recently developed a light-field tomographic FLIM (LIFT-FLIM) approach [50], which eliminates the necessity for sample rotation and enables 3D FLIM of biological samples with micron-scale resolution.

Sharing its roots with optical tomography, LIFT-FLIM acquires multiple views of a 3D object and determines depth information through tomographic reconstruction [51,52] (Fig. 4e). A distinctive feature of LIFT-FLIM lies in its approach: instead of rotating the sample, it scans the system pupil to gather angular information while maintaining the sample in a static position. Moreover, unlike the conventional method of directly capturing a 2D perspective image at each view angle, LIFT-FLIM opts for measuring only the en-face projections of the image. This unique approach transforms 2D perspective images into lines, enabling the mapping of high-dimensional optical information to a low-dimensional space through pure optical operations.

This dimensionality reduction proves particularly beneficial for ultrafast image sensors, which are inherently favored for fabrication in a low-dimensional format [53]. For example, when monolithic SPAD arrays are fabricated in 2D format, the native fill factor is typically low due to physical constraints imposed by intricate timing electronics at each pixel, particularly in the TCSPC mode. In contrast, a linear SPAD array offers a significantly higher fill factor by placing light-sensitive regions in close proximity, allowing for a substantial increase in light throughput. This advantageous arrangement permits the positioning of timing electronics above or below the pixel area. Additionally, the fabrication cost of a linear SPAD array is considerably lower than its 2D counterpart, rendering it more accessible for routine lab applications. In LIFT-FLIM, we take advantage of this transformation by directly capturing 1D projection images using a linear SPAD array, allowing for 3D fluorescence lifetime imaging with exceptional single-photon sensitivity (Fig. 4f).

In addition to its 3D imaging capabilities, LIFT-FLIM exhibits inherent compatibility with spectral imaging. Exploiting this attribute, we expanded the system’s functionality to incorporate spectral FLIM (sFLIM). This was accomplished by dispersing the 1D projection images through a diffraction grating, followed by feeding the resulting image into a time-gated camera for precise lifetime measurement. This approach facilitates the simultaneous acquisition of 3D FLIM images at multiple wavelengths, establishing LIFT-FLIM as a versatile tool for comprehensive analysis of both lifetime and spectral information.

5. Perspectives

The toolbox for high-speed and 3D FLIM has been ever expanding. We envision that advancements will derive substantial benefits from progress in the following three key technical areas.

5.1. Computational imaging

FLIM has long relied solely on hardware to fulfill its imaging function. However, this image acquisition paradigm faces significant limitations. 3D FLIM essentially measures a five-dimensional datacube (x, y, z, τ, t) (x, y, z, spatial coordinates; τ, fluorescence lifetime; t, time). The space-bandwidth-time-product of the imaging system inherently constrains the information flux captured, resulting in an unavoidable trade-off between the imaging volume, spatial resolution, lifetime accuracy, and frame rate [54]. Moreover, the information acquired is frequently redundant for practical tasks such as lifetime unmixing and ratiometric calculations, posing challenges in data transmission, storage, and processing.

Recent breakthroughs in artificial intelligence (AI), particularly deep learning, have ushered in transformative solutions to address these challenges [55–57]. The integration of AI into FLIM has given rise to a hybrid imaging modality known as computational FLIM. This innovative approach transcends the constraints of conventional FLIM methods by replacing, in part or entirely, the physical layer with a digital counterpart. For instance, Sorrells et al. have devised a computational method that replaces conventional constant fraction discriminator circuits in single photon counting devices [58]. This replacement enhances the accuracy and speed of lifetime measurements. In another noteworthy example, Ochoa et al. engineered a deep-learning-based single-pixel TCSPC camera for widefield FLIM imaging [59,60](Fig. 5a). The dimensional gap between the point detector and the target 2D FLIM image is bridged through a neural-network-driven optical encoding scheme, diverging from the conventional physical scanning method. This innovation facilitates wide-field FLIM imaging with a remarkable data compression ratio of up to 99 %, thereby significantly alleviating the generated data load (Fig. 5b).

Moreover, the physical and digital layers of a computational FLIM system can be harmoniously co-optimized to improve imaging performance. The core idea is to make the measurement model a trainable parameter that can be optimized with training data and then use back-propagation to fine tune the hardware for improved spatiotemporal resolutions. For example, in the context of LIFT-FLIM [50], the digital layer can be managed through an end-to-end optimization model, leveraging back propagation to determine the optimal projection measurement angle at each sub-pupil location. This, in turn, aids in selecting the optimal locations within the object’s frequency space to be sampled. Through this joint optimization approach, diverse depth-dependent point spread functions can be generated, contributing to the creation of optimal 3D lifetime image reconstructions.

5.2. Advanced detector technologies

Traditional FLIM systems typically rely on photomultiplier tubes and micro-channel plates for recording fluorescence lifetime. However, these components have several drawbacks,

such as their vacuum-based operation, susceptibility to magnetic fields, and the need for high voltage. These limitations hinder the widespread adoption of these sensors in high-resolution arrays for parallel lifetime measurements.

The advent of SPADs marks a transformative shift in FLIM technology [26]. SPADs, being solid-state devices, can operate in normal atmospheric conditions at room temperature, offering single-photon detection and photon-counting capabilities. Notably, the integration of SPADs into standard CMOS technology allows for the incorporation of electronic circuits on the same silicon chip as the detectors. This advancement paves the way for high-volume production of single-photon detectors for cost-effective FLIM implementations. Despite these advantages, the monolithic integration of SPADs in CMOS has presented challenges, including a loss of photon sensitivity due to a low fill factor (typically < 10 %) and time-resolution nonuniformity arising from the intense sharing of time-resolved circuitry.

Recent developments in 3D-stacked CMOS technology represent an evolution from 2D CMOS for SPADs [53,61]. The primary benefit of 3D-stacked chips lies in their potential for advanced functionality, lower power consumption, increased fill factor, improved near-infrared sensitivity, and enhanced timing performance. In the 3D-stacked approach, SPADs are implemented in the top-tier chip, crafted through an advanced CMOS image sensor process. Simultaneously, the bottom-tier chip, typically constructed with an even more advanced CMOS technology, accommodates all the circuits for data processing, compression, and communication. Moreover, the utilization of a smaller pitch in 3D-stacked CMOS technology stands out as the pivotal solution for achieving high-performance multi-megapixel SPAD sensors. For example, Hutchings et al. developed a 3D-stacked SPAD image sensor with 256×256 pixels with a 51 % fill factor and demonstrated its application in time-of-flight imaging [62]. The same group later engineered another 3D-stacked SPAD image sensor with 128×120 pixels and a 45 % fill factor for FLIM endomicroscopy [63,64] (Fig. 5c, d).

5.3. Deep tissue imaging

Optical scattering poses a persistent challenge in optical imaging. The limited imaging depth of visible light within biological tissues, typically confined to a few hundred microns, has been a major bottle-neck for translating 3D FLIM for clinical applications. However, there is a promising avenue that involves employing longer optical wavelengths, particularly in the near-infrared (NIR) (700–900 nm) and NIR-II (1000–2000 nm) spectral window, where tissue scattering decreases significantly.

Capitalizing on the advantages offered by the low-scattering NIR spectral window, FLIM has traditionally been integrated with two-photon fluorescence microscopy to facilitate deep tissue imaging [14]. However, the conventional two-photon FLIM microscopes face challenges, as their extensive scanning requirements and the low two-photon absorption cross sections of fluorophores result in slower frame rates even compared to confocal FLIM, making them impractical for achieving dense depth samplings in 3D FLIM. In response to this issue, recent endeavors have focused on integration of FLIM with wide-field two-photon excitation techniques like temporal focusing [65]. This strategic combination

enables the parallel acquisition of in-plane fluorescence lifetimes, significantly enhancing the acquisition speed.

The imaging depth of 3D FLIM can be further extended by using light of longer wavelengths in the NIR-II (also referred to as short-wave near-infrared) range (Fig. 5e). Compared to visible and NIR-I imaging, The NIR-II window offers significantly improved signal-to-background ratios and penetration depth, boasting up to a 1000-fold reduction in photon scattering [66–68]. It holds the potential for achieving micron-scale imaging resolution and penetrating tissue depths of several centimeters, rendering it a highly valuable tool for deep tissue imaging. In particular, recent studies have unveiled that many established NIR-I fluorophores can double as effective contrast agents in NIR-II FLIM imaging, courtesy of their long-tailed spectral emissions [69,70] (Fig. 5f). This revelation immediately benefits various preclinical and clinical FLIM applications.

It's noteworthy that existing SPADs, predominantly made of all-silicon, conventionally operate at wavelengths below 1 μm. To facilitate photon-counting FLIM within the NIR-II range, a promising alternative lies in the use of Germanium-on-silicon (Ge-on-Si) SPAD detectors [71]. These detectors not only offer high sensitivity but also provide picosecond resolution timing measurements for NIR-II photons, overcoming the limitations of traditional SPADs and paving the way for enhanced FLIM imaging capabilities in this critical wavelength range.

In addition to employing longer-wavelength light, an alternative strategy for achieving deep-tissue FLIM involves integrating it with diffuse optical tomography (DOT) [72]. Traditional FLIM is primarily designed for ballistic imaging, often overlooking optical scattering. In contrast, DOT-FLIM expands the possibilities of lifetime imaging into the optical diffusive regime by employing mathematical models to describe light propagation in tissues and solving the corresponding inverse problem [45,73,74]. Despite its advancements, DOT-FLIM, much like conventional DOT techniques, suffers from a poor spatial resolution. A potential avenue for improvement lies in synergizing DOT-FLIM with time-domain methodologies, particularly leveraging early-arrival photons [75–77].

Acknowledgements

This work was supported by the National Institutes of Health [R01HL165318, RF1NS128488]

Data availability

No data was used for the research described in the article.

References

[1]. Berezin MY, Achilefu S, Fluorescence lifetime measurements and biological imaging, Chem. Rev 110 (2010) 2641–2684. [PubMed: 20356094]

[2]. Datta R, Heaster TM, Sharick JT, Gillette AA, Skala MC, Fluorescence lifetime imaging microscopy: fundamentals and advances in instrumentation, analysis, and applications, J. Biomed. Opt 25 (2020) 071203. [PubMed: 32406215]

[3]. Alfonso-Garcia A, Bec J, Weyers B, Marsden M, Zhou X, Li C, Marcu L, Mesoscopic fluorescence lifetime imaging: fundamental principles, clinical applications and future directions, J. Biophotonics 14 (2021) e202000472.

[4]. Dmitriev RI, Intes X, Barroso MM, Luminescence lifetime imaging of three-dimensional biological objects, J. Cell Sci 134 (2021) 1–17. [PubMed: 33961054]

[5]. Le Marois A, Suhling K, Quantitative live cell FLIM imaging in three dimensions, Multi-Parametric Live Cell Microscopy of 3D Tissue Models (2017) 31–48.

[6]. Becker W, Fluorescence lifetime imaging – techniques and applications, J. Microsc 247 (2012) 119–136. [PubMed: 22621335]

[7]. Borst JW, Visser AJWG, Fluorescence lifetime imaging microscopy in life sciences, Meas. Sci. Technol 21 (2010) 102002.

[8]. Ebrecht R, Don Paul C, Wouters FS, Fluorescence lifetime imaging microscopy in the medical sciences, Protoplasma 251 (2014) 293–305. [PubMed: 24390249]

[9]. Marcu L, Fluorescence lifetime techniques in medical applications, Ann. Biomed. Eng 40 (2012) 304–331. [PubMed: 22273730]

[10]. Marcu L, French PMW, Elson DS, Fluorescence lifetime spectroscopy and imaging : principles and applications in biomedical diagnostics, CRC Press/Taylor & Francis Group, Boca Raton, 2014.

[11]. Eichorst JP, Teng KW, Clegg RM: Fluorescence lifetime imaging techniques: Frequency-domain FLIM. In Fluorescence Lifetime Spectroscopy and Imaging: Principles and Applications in Biomedical Diagnostics. Edited by Marcu L F P, and Elson DS CRC Press; 2014:165–186.

[12]. Becker W: Fluorescence lifetime imaging techniques: time-correlated single-photon counting. In Fluorescence Lifetime Spectroscopy and Imaging. Edited by: CRC Press; 2014:220–251.

[13]. McGinty J, Dunsby C, French PM, Fluorescence lifetime imaging techniques: time-gated fluorescence lifetime imaging, in: Marcu L (Ed.), Fluorescence Lifetime Spectroscopy and Imaging, CRC Press, PF aDEC, 2014, pp. 187–199.

[14]. Gratton E, Breusegem S, Sutin J, Ruan QQ, Fluorescence lifetime imaging for the two-photon microscope: time-domain and frequency-domain methods, J. Biomed. Opt 8 (2003) 381–390. [PubMed: 12880343]

[15]. Hopt A, Neher E, Highly nonlinear photodamage in two-photon fluorescence microscopy, Biophys. J 80 (2001) 2029–2036. [PubMed: 11259316]

[16]. Visscher K, Brakenhoff GJ, Visser TD, Fluorescence saturation in confocal microscopy, J. Microscopy-Oxford 175 (1994) 162–165.

[17]. Liu X, Lin D, Becker W, Niu J, Yu B, Liu L, Qu J, Fast fluorescence lifetime imaging techniques: a review on challenge and development, J. Innovative Optical Health Sci 12 (2019) 1930003.

[18]. Becker W, The bh TCSPC handbook, 10th edition:, Becker & Hickl GmbH, 2023.

[19]. Becker W, Advanced time-correlated single photon counting techniques, Springer, Berlin; New York, 2005.

[20]. Pawley JB, Handbook of biological confocal microscopy edn 3rd, Springer, New York, NY, 2006.

[21]. Becker W, Bergmann A, Smietana S, Fast-acquisition TCSPC FLIM with sub-25-ps IRF width, Multiphoton Microscopy in the Biomedical Sci. XIX: SPIE (2019) 1088206.

[22]. Liu S, Zhang Z, Zheng J, Xu L, Kuang C, Liu X, Parallelized fluorescence lifetime imaging microscopy (FLIM) based on photon reassignment, Opt. Commun 421 (2018) 83–89.

[23]. Bower AJ, Li J, Chaney EJ, Marjanovic M, Spillman DR, Boppart SA, High-speed imaging of transient metabolic dynamics using two-photon fluorescence lifetime imaging microscopy, Optica 5 (2018) 1290–1296. [PubMed: 30984802]

[24]. Bower AJ, Sorrells JE, Li J, Marjanovic M, Barkalifa R, Boppart SA, Tracking metabolic dynamics of apoptosis with high-speed two-photon fluorescence lifetime imaging microscopy, Biomed. Opt. Express 10 (2019) 6408–6421. [PubMed: 31853407]

[25]. Karpf S, Riche CT, Di Carlo D, Goel A, Zeiger WA, Suresh A, Portera-Cailliau C, Jalali B, Spectro-temporal encoded multiphoton microscopy and fluorescence lifetime imaging at kilohertz frame-rates, Nat. Commun 11 (2020) 2062. [PubMed: 32346060]

[26]. Bruschini C, Homulle H, Antolovic IM, Burri S, Charbon E, Single-photon avalanche diode imagers in biophotonics: review and outlook, Light Sci. Appl 8 (2019) 87. [PubMed: 31645931]

[27]. Zickus V, Wu M-L, Morimoto K, Kapitany V, Fatima A, Turpin A, Insall R, Whitelaw J, Machesky L, Bruschini C, Fluorescence lifetime imaging with a megapixel SPAD camera and neural network lifetime estimation, Sci. Rep 10 (2020) 20986. [PubMed: 33268900]

[28]. Morimoto K, Ardelean A, Wu M-L, Ulku AC, Antolovic IM, Bruschini C, Charbon E, Megapixel time-gated SPAD image sensor for 2D and 3D imaging applications, Optica 7 (2020) 346–354.

[29]. Kapitany V, Zickus V, Fatima A, Carles G, Faccio D, Single-shot time-folded fluorescence lifetime imaging, Proc. Natl. Acad. Sci 120 (2023) e2214617120.

[30]. Ma Y, Lee Y, Best-Popescu C, Gao L, High-speed compressed-sensing fluorescence lifetime imaging microscopy of live cells, Proc. Natl. Acad. Sci 118 (2021) e2004176118.

[31]. Gao L, Liang J, Li C, Wang LV, Single-shot compressed ultrafast photography at one hundred billion frames per second, Nature 516 (2014) 74–77. [PubMed: 25471883]

[32]. Liu X, Liu J, Jiang C, Vetrone F, Liang J, Single-shot compressed optical-streaking ultra-high-speed photography, Opt. Lett 44 (2019) 1387–1390. [PubMed: 30874657]

[33]. Liu X, Skripka A, Lai Y, Jiang C, Liu J, Vetrone F, Liang J, Fast wide-field upconversion luminescence lifetime thermometry enabled by single-shot compressed ultrahigh-speed imaging, Nat. Commun 12 (2021) 6401. [PubMed: 34737314]

[34]. Bowman AJ, Klopfer BB, Juffmann T, Kasevich MA, Electro-optic imaging enables efficient wide-field fluorescence lifetime microscopy, Nat. Commun 10 (2019) 4561. [PubMed: 31594938]

[35]. Bowman AJ, Kasevich MA, Resonant electro-optic imaging for microscopy at Nanosecond resolution, ACS Nano 15 (2021) 16043–16054. [PubMed: 34546704]

[36]. Bowman AJ, Huang C, Schnitzer MJ, Kasevich MA, Wide-field fluorescence lifetime imaging of neuron spiking and subthreshold activity in vivo, Sci 380 (2023) 1270–1275.

[37]. Grant D, Elson D, Schimpf D, Dunsby C, Requejo-Isidro J, Auksorius E, Munro I, Neil M, French P, Nye E, Optically sectioned fluorescence lifetime imaging using a nipkow disk microscope and a tunable ultrafast continuum excitation source, Opt. Lett 30 (2005) 3353–3355. [PubMed: 16389829]

[38]. Grant DM, McGinty J, McGhee E, Bunney T, Owen D, Talbot C, Zhang W, Kumar S, Munro I, Lanigan P, High speed optically sectioned fluorescence lifetime imaging permits study of live cell signaling events, Opt. Express 15 (2007) 15656–15673. [PubMed: 19550853]

[39]. Görlitz F, Corcoran DS, Garcia Castano EA, Leitinger B, Neil MA, Dunsby C, French PM, Mapping molecular function to biological nanostructure: combining structured illumination microscopy with fluorescence lifetime imaging (SIM+ FLIM), MDPI, In Photonics, 2017, p. 40.

[40]. Mitchell CA, Poland SP, Seyforth J, Nedbal J, Gelot T, Huq T, Holst G, Knight RD, Ameer-Beg SM, Functional in vivo imaging using fluorescence lifetime light-sheet microscopy, Opt. Lett 42 (2017) 1269–1272. [PubMed: 28362747]

[41]. Funane T, Hou SS, Zoltowska KM, van Veluw SJ, Berezovska O, Kumar AT, Bacskai BJ, Selective plane illumination microscopy (SPIM) with time-domain fluorescence lifetime imaging microscopy (FLIM) for volumetric measurement of cleared mouse brain samples, Rev. Sci. Instrum 89 (2018).

[42]. Hirvonen LM, Nedbal J, Almutairi N, Phillips TA, Becker W, Conneely T, Milnes J, Cox S, Stürzenbaum S, Suhling K, Lightsheet fluorescence lifetime imaging microscopy with wide-field time-correlated single photon counting, J. Biophotonics 13 (2020) e201960099.

[43]. Samimi K, Desa DE, Lin W, Weiss K, Li J, Huisken J, Miskolci V, Huttenlocher A, Chacko JV, Velten A, et al. : Light sheet autofluorescence lifetime imaging with a single photon avalanche diode array. bioRxiv 2023.

[44]. Greger K, Neetz MJ, Reynaud EG, Stelzer EH, Three-dimensional fluorescence lifetime imaging with a single plane illumination microscope provides an improved signal to noise ratio, Opt. Express 19 (2011) 20743–20750. [PubMed: 21997084]

[45]. Kumar AT: Tomographic fluorescence lifetime imaging. In Fluorescence Lifetime Spectroscopy and Imaging. Edited by: CRC Press; 2014:461–476.

[46]. McGinty J, Tahir KB, Laine R, Talbot CB, Dunsby C, Neil MA, Quintana L, Swoger J, Sharpe J, French PM, Fluorescence lifetime optical projection tomography, J Biophotonics 1 (2008) 390–394. [PubMed: 19343662]

[47]. McGinty J, Taylor HB, Chen L, Bugeon L, Lamb JR, Dallman MJ, French PMW, In vivo fluorescence lifetime optical projection tomography, Biomed. Opt. Express 2 (2011) 1340–1350. [PubMed: 21559145]

[48]. Andrews N, Ramel M-C, Kumar S, Alexandrov Y, Kelly DJ, Warren SC, Kerry L, Lockwood N, Frolov A, Frankel P, et al. , Visualising apoptosis in live zebrafish using fluorescence lifetime imaging with optical projection tomography to map FRET biosensor activity in space and time, J. Biophotonics 9 (2016) 414–424. [PubMed: 26753623]

[49]. Sun J, Zhao F, Zhu L, Liu B, Fei P, Optical projection tomography reconstruction with few views using highly-generalizable deep learning at sinogram domain, Biomed. Opt. Express 14 (2023) 6260–6270. [PubMed: 38420331]

[50]. Ma Y, Huang L, Sen C, Burri S, Bruschini C, Yang X, Cameron R, Fishbein G, Gomperts BN, Ozcan A, et al. , Light-field tomographic fluorescence lifetime imaging microscopy, PREPRINT at Res. Square (2023).

[51]. Feng X, Gao L, Ultrafast light field tomography for snapshot transient and non-line-of-sight imaging, Nat. Commun 12 (2021) 2179. [PubMed: 33846338]

[52]. Feng X, Ma Y, Gao L, Compact light field photography towards versatile three-dimensional vision, Nat. Commun 13 (2022) 3333. [PubMed: 35680933]

[53]. Hirvonen LM, Suhling K, Fast timing techniques in FLIM applications, Front. Phys 8 (2020) 161.

[54]. Park J, Brady DJ, Zheng G, Tian L, Gao L, Review of bio-optical imaging systems with a high space-bandwidth product, Adv. Photonics 3 (2021) 044001. [PubMed: 35178513]

[55]. Wetzstein G, Ozcan A, Gigan S, Fan S, Englund D, Soljačíc M, Denz C, Miller DAB, Psaltis D, Inference in artificial intelligence with deep optics and photonics, Nature 588 (2020) 39–47. [PubMed: 33268862]

[56]. Tian L, Hunt B, Bell MAL, Yi J, Smith JT, Ochoa M, Intes X, Durr NJ, Deep Learning in biomedical optics, Lasers Surg. Med 53 (2021) 748–775. [PubMed: 34015146]

[57]. Brady DJ, Fang L, Ma Z, Deep learning for camera data acquisition, control, and image estimation, Adv. Opt. Photon 12 (2020) 787–846.

[58]. Sorrells JE, Iyer RR, Yang L, Chaney EJ, Marjanovic M, Tu H, Boppart SA, Single-photon peak event detection (SPEED): a computational method for fast photon counting in fluorescence lifetime imaging microscopy, Opt. Express 29 (2021) 37759–37775. [PubMed: 34808842]

[59]. Ochoa M, Rudkouskaya A, Yao R, Yan P, Barroso M, Intes X, High compression deep learning based single-pixel hyperspectral macroscopic fluorescence lifetime imaging in vivo, Biomed. Opt. Express 11 (2020) 5401–5424. [PubMed: 33149959]

[60]. Pian Q, Yao R, Sinsuebphon N, Intes X, Compressive hyperspectral time-resolved wide-field fluorescence lifetime imaging, Nat. Photonics 11 (2017) 411–414. [PubMed: 29242714]

[61]. Lee M-J, Charbon E, Progress in single-photon avalanche diode image sensors in standard CMOS: from two-dimensional monolithic to three-dimensional-stacked technology, Jpn. J. Appl. Phys (2018).

[62]. Hutchings SW, Johnston N, Gyongy I, Al Abbas T, Dutton NA, Tyler M, Chan S, Leach J, Henderson RK, A reconfigurable 3-D-stacked SPAD imager with in-pixel histogramming for flash LIDAR or high-speed time-of-flight imaging, IEEE J. Solid State Circuits 54 (2019) 2947–2956.

[63]. Erdogan AT, Al Abbas T, Finlayson N, Hopkinson C, Gyongy I, Almer O, Dutton NA, Henderson RK, A high dynamic range 128 × 120 3-D stacked CMOS SPAD image sensor SoC for fluorescence microendoscopy, IEEE J. Solid State Circuits 57 (2022) 1649–1660.

[64]. Matheson AB, Erdogan AT, Hopkinson C, Borrowman S, Loake GJ, Tanner MG, Henderson RK, Handheld wide-field fluorescence lifetime imaging system based on a distally mounted SPAD array, Opt. Express 31 (2023) 22766–22775. [PubMed: 37475380]

[65]. Choi H, Tzeranis DS, Cha JW, Clémenceau P, de Jong SJ, van Geest LK, Moon JH, Yannas IV, So PT, 3D-resolved fluorescence and phosphorescence lifetime imaging using temporal focusing wide-field two-photon excitation, Opt. Express 20 (2012) 26219–26235. [PubMed: 23187477]

[66]. Jia S, Sletten EM, Spatiotemporal control of biology: synthetic photochemistry toolbox with far-red and near-infrared light, ACS Chem. Biol 17 (2021) 3255–3269. [PubMed: 34516095]

[67]. Wong KC, Sletten EM, Extending optical chemical tools and technologies to mice by shifting to the shortwave infrared region, Curr. Opin. Chem. Biol 68 (2022) 102131. [PubMed: 35366502]

[68]. Cao J, Zhu B, Zheng K, He S, Meng L, Song J, Yang H, Recent progress in NIR-II contrast agent for biological imaging, Front. Bioeng. Biotechnol 7 (2020) 487. [PubMed: 32083067]

[69]. Carr JA, Franke D, Caram JR, Perkinson CF, Saif M, Askoxylakis V, Datta M, Fukumura D, Jain RK, Bawendi MG, Shortwave infrared fluorescence imaging with the clinically approved near-infrared dye indocyanine green, Proc. Natl. Acad. Sci 115 (2018) 4465–4470. [PubMed: 29626132]

[70]. Chavez L, Gao S, Intes X, Characterization of fluorescence lifetime of organic fluorophores for molecular imaging in the shortwave infrared window, J. Biomed. Opt 28 (2023) 094806.

[71]. Thorburn F, Yi X, Greener ZM, Kirdoda J, Millar RW, Huddleston LL, Paul DJ, Buller GS, Ge-on-si single-photon avalanche diode detectors for short-wave infrared wavelengths, J. Phy: Photonics 4 (2022) 012001.

[72]. Boas DA, Brooks DH, Miller EL, DiMarzio CA, Kilmer M, Gaudette RJ, Zhang Q, Imaging the body with diffuse optical tomography, IEEE Signal Process Mag 18 (2001) 57–75.

[73]. Kumar AT, Raymond SB, Dunn AK, Bacskai BJ, Boas DA, A time domain fluorescence tomography system for small animal imaging, IEEE Trans. Med. Imaging 27 (2008) 1152–1163. [PubMed: 18672432]

[74]. Nothdurft RE, Patwardhan SV, Akers W, Ye Y, Achilefu S, Culver JP, In vivo fluorescence lifetime tomography, J. Biomed. Opt (2009).

[75]. Chen K, Perelman LT, Zhang Q, Dasari RR, Feld MS, Optical computed tomography in a turbid medium using early arriving photons, J. Biomed. Opt 5 (2000) 144–155. [PubMed: 10938778]

[76]. Liu F, Yoo K, Alfano RR, Ultrafast laser-pulse transmission and imaging through biological tissues, Appl. Opt 32 (1993) 554–558. [PubMed: 20802724]

[77]. Niedre MJ, de Kleine RH, Aikawa E, Kirsch DG, Weissleder R, Ntziachristos V, Early photon tomography allows fluorescence detection of lung carcinomas and disease progression in mice in vivo, Proc. Natl. Acad. Sci 105 (2008) 19126–19131. [PubMed: 19015534]

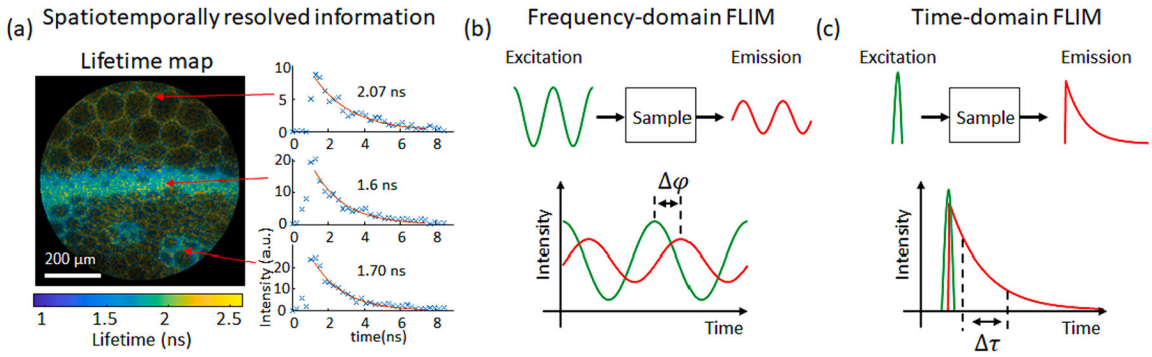

Fig. 1. Fluorescence lifetime imaging.

(a) FLIM records time-resolved fluorescence decay at each spatial location. (b) Frequency-domain FLIM. (c) Time-domain FLIM.

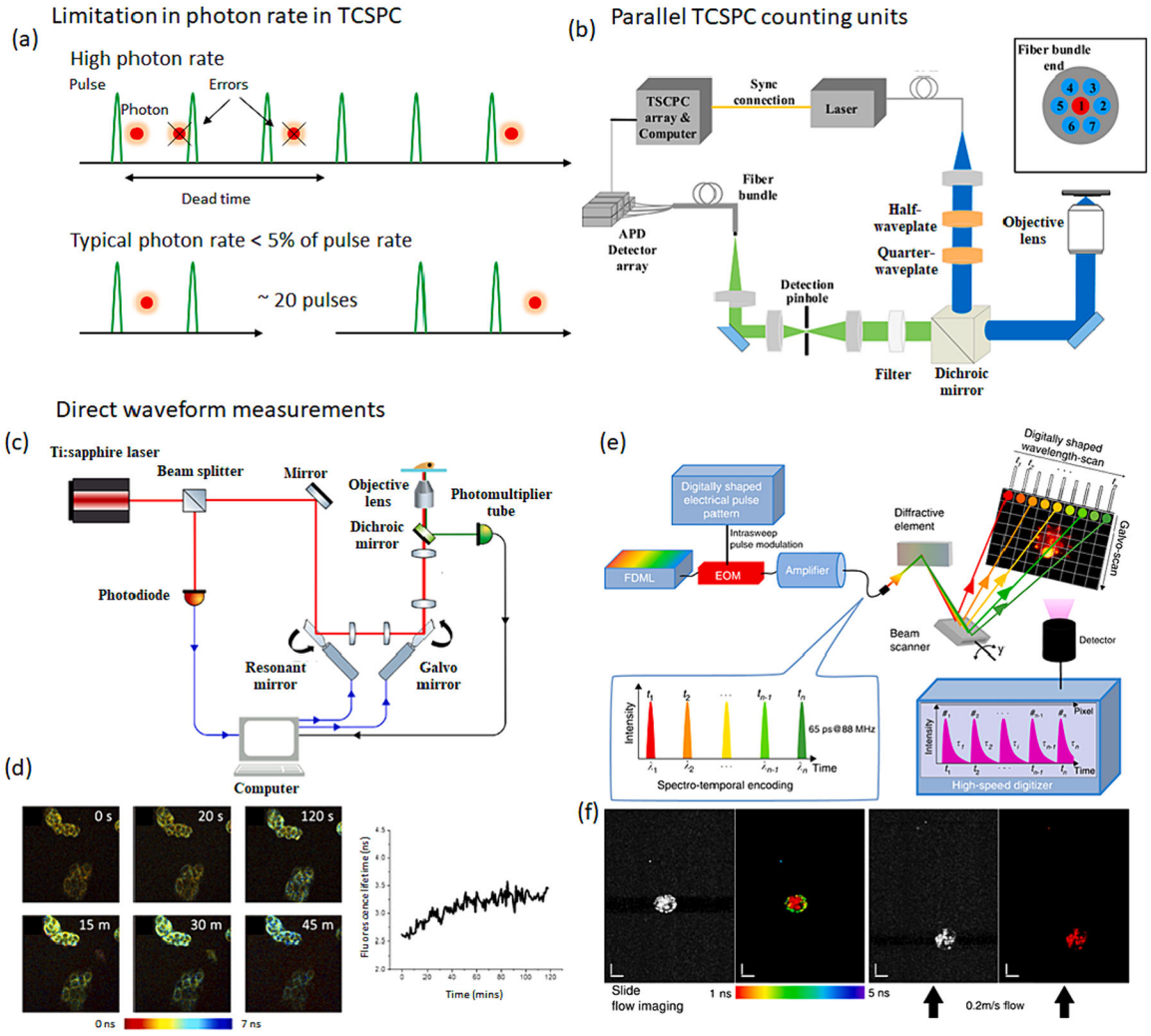

Fig. 2.

High-speed FLIM methods. (a) The photon rate (throughput) of TCSPC-mode FLIM is limited to avoid measurement errors such as pile-up effects and counting loss. (b) The photon rate can be increased by using TCSPC with parallel detector arrays [22]. (c) Fluorescence decay waveform can be directly measured by high-speed photodetectors [23]. (d) Two-photon fluorescence lifetime dynamics of apoptosis induced cells were recorded at a video rate [24]. (e) Spectro-temporal encoded illumination enables kilohertz FLIM [25] and its application in (f) imaging flow cytometry.

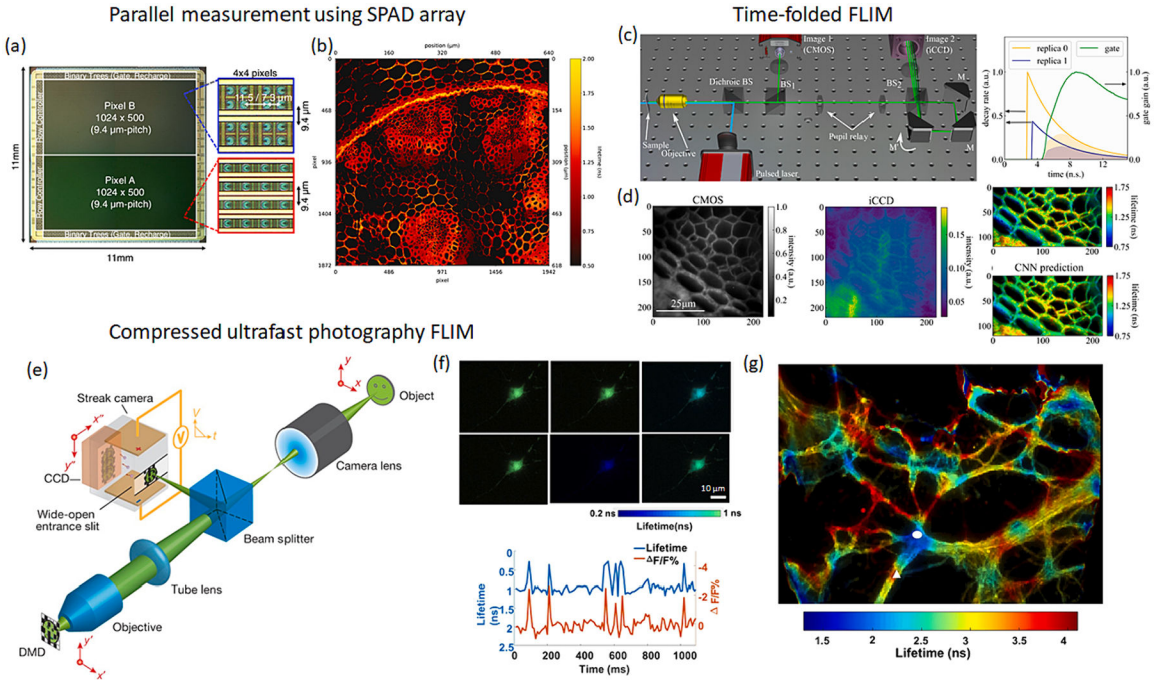

Fig. 3.

High-speed FLIM methods using 2D detector arrays. (a) 0.5-megapixel SPAD camera with an acquisition rate up to 1 Hz [28] (b) 3.6 megapixel wide-field FLIM image captured by using the SPAD camera with image stitching [27]. (c) Time-folded FLIM. An optical cavity generates temporally delayed and spatially sheared replicas of fluorescent decay signal [29]. (d) The signal from the CMOS sensor and intensified CCD was used to generate fluorescence lifetime image with either an inverse retrieval method or neural network [29]. (e) Compressed ultrafast photography FLIM. The fluorescence signal is spatially mapped by the DMD, temporally sheared by the streak camera, and mapped onto the CCD sensor [31]. The fluorescence lifetime image is computationally reconstructed by solving the inverse problem. (f) High-speed fluorescence lifetime imaging of neural action potentials in live cells [30]. (g) Fluorescence lifetime imaging of neuronal cytoskeleton immunolabeled with multiple fluorophores.

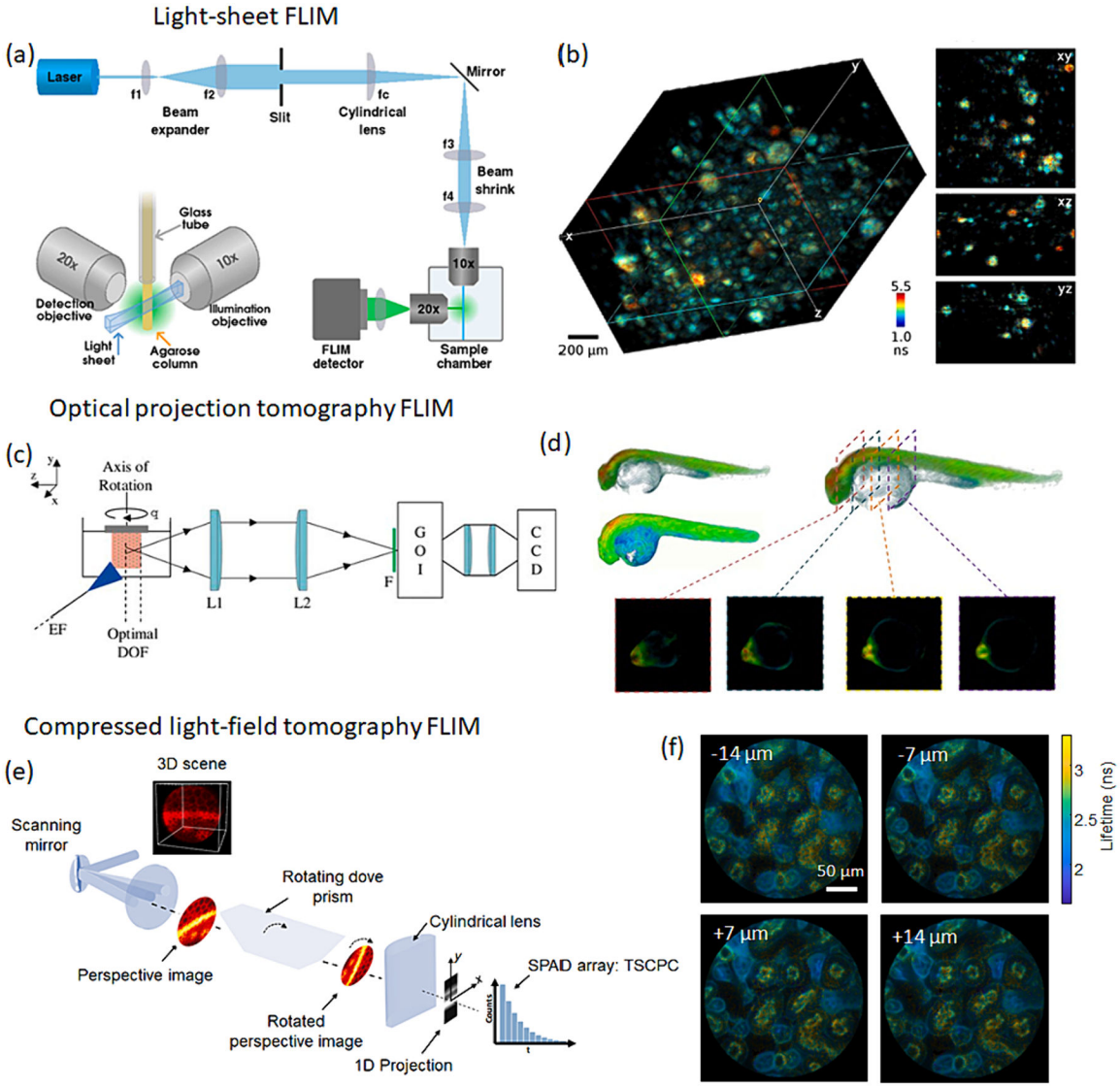

Fig. 4.

3D FLIM. (a) Light-sheet microscopy with a TCSPC-based wide-field FLIM detector [42]. (b) 3D volumetric fluorescence lifetime image of a mixture of fluorescent beads and quantum dots [42]. (c) 3D fluorescence lifetime imaging with optical projection tomography. A series of time-gated fluorescence images were acquired at various projection angles by rotating the sample [46]. (d) 3D volumetric fluorescence lifetime image of a live zebrafish [48]. (e) Light-field tomography FLIM. The 2D perspective images of a 3D sample are captured by pupil selection through a scanning mirror. The resultant images are further rotated and compressed along one spatial axis by a dove prism and cylindrical lens, respectively. (f) High-resolution depth-sectioned fluorescence lifetime images of a mouse kidney tissue section.

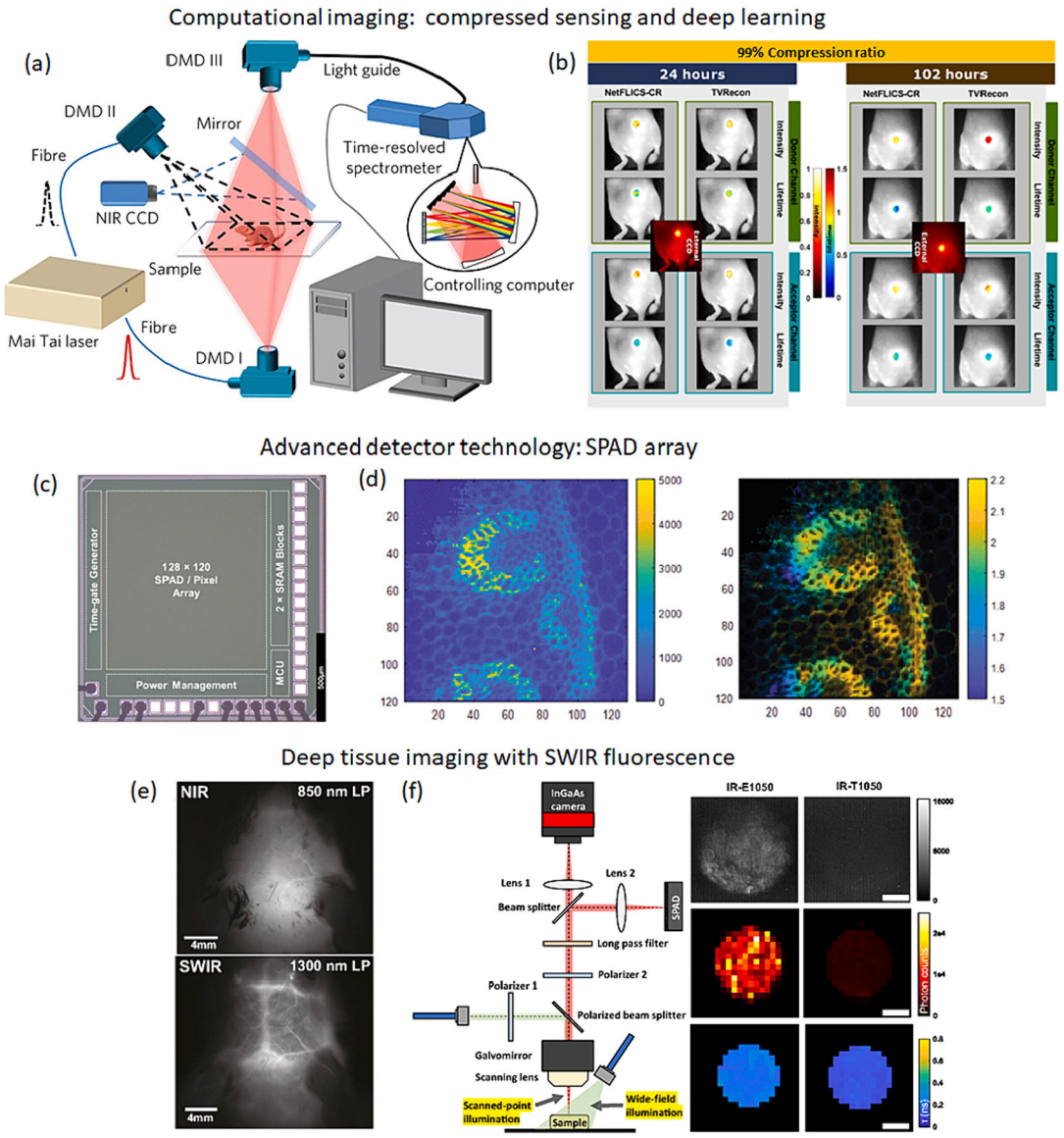

Fig. 5.

Future perspective. (a) Compressed sensing method to overcome the information limit in FLIM [60]. (b) In vivo FLIM with a data compression ratio of 99% [59]. (c) 3D-stacked SPAD image sensor with a 45% fill factor [63]. (d) Fluorescence lifetime imaging of Convallaria Majalis sample at a video rate using the SPAD array [63]. (e) The mouse brain vasculature imaging through skin and skull. SWIR fluorescence enables deep tissue imaging beyond the NIR window [69]. (f) Lifetime characterization of SWIR fluorophores [70].